Modeling of a Novel Microstrip Ring Resonator for Wireless Applications

Seyi Stephen Olokede and Babu Sena Paul
Department of Electrical & Electronic Engineering Technology
University of Johannesburg, Doornfontein, Johannesburg 2028, South Africa

Abstract— In this paper, we present the modeling of the microstrip ring resonator (MRR) for wireless applications. The proposed MRR is designed to operate at 5.8 GHz using a combination of two sub-wavelength ($\lambda/4$) bent MRRs together with two ($\lambda/8$) arms to form a half ring of $\lambda/2$ in length. The combined structure is excited by an end-coupled transmission line in such a way as to center couple the two half rings. The entire structure is modeled numerically using an equivalent circuit that was derived, and hence characterized with the aid of the 2D equivalent circuit modeler. The effects of the various gap capacitances on the reflection coefficients, insertion loss, resonant frequency and bandwidth are investigated.

1. INTRODUCTION

One notable attraction of microstrip ring resonators (MRRs) that distinguish them is their ability to satisfy the increasing need for the optimum usage of space in modern microwave circuits. Low cost, high quality (Q) and low radiation loss for wireless communication are added advantages. It is therefore not uncommon to find various ring resonator designs owing to some specific advantages of compact size [1–3], high Q and possible suitability for a narrow-band range of applications, having typically less than 5% bandwidth [4]. Usually, the end-coupled structures are favorite ways of designing new resonators because of their size advantage, lightweight, low cost, inherent good ability to stop or pass a certain frequency band [5] and ease of fabrication [6], though with a characteristic high insertion loss. This is responsible for their narrow bandwidth peculiarities [7]. As a result of their advantageous features, many other resonator topologies designed on the basis of MRR structure are ubiquitous [8, 9]. However, interactions between these lumped components have been difficult to analyze in order to achieve accurate characterization. This is because an ideal sub-wavelength linear impedance section is not realizable at lower frequencies because of fringing fields, particularly by virtue of their electrical and physical lengths. Hence, such components store or release electric and magnetic energies across them and their resistance accounts for the dissipated power. To underpin their electrical behavior adequately, the proposed model is investigated.

2. THE MODEL

The proposed structure is as shown in Figure 1 and its parameter definition is as stated in Table 1. The edge gap, k of the proposed model was optimized to determine the bandwidth of the resonator. The parameter r is the radius of the MRR, whereas ℓ is the circumference of each MRR. The resonant frequency of the resonator can be varied by varying the radius r of the MRR, and also the edge gap k. The resonance capacitance can also be increased by increasing the width of the resonator. As a result, the proposed MRR becomes more compact when the resonant frequency is further reduced by extending the conductor length. For instance, the resonance of each half MRR at circumferential length (ℓ) is higher than at ($\ell + n$), and much higher than at aperture length ($\ell + n + m$), as demonstrated in Figure 1, without any additional area occupation. Alternatively, the aperture size, and hence the area occupation of the proposed model, are the same at $\ell = \lambda/4$ as at $\ell = \lambda/4 + n$ and $\ell = \lambda/4 + n + m$, though with varying resonance frequencies. Hence, the effective area occupation is $\ell = \lambda/4$ even though each half MRR is more than approximately a wavelength long with the aperture size equal to ($\ell + n + m$). This is the very reason for the compact capability of the proposed model. The equivalent circuit of each half MRR is shown in Figure 2 [10]. The proposed resonator can be modeled by a single parallel RLC resonator circuit. The operational dynamic of the equivalent circuit cannot only reduce the length of the open transmission line resonator, but can also shift the spurious response of an open transmission

Table 1: Proposed parameter definitions.

Parameters Definitions	Notations	Values (mm)
Length of Each MRR	ℓ	$\lambda/4$
Half Feedline Length	ℓ_1	2.8
Half Feedline Matching Length	ℓ_2	2.0
End-coupled Termination Length	ℓ_3	4.0
Conductor Head	m	1.2
Conductor Arm	n	$\lambda/8$
Conductor Head Width	w	0.3
Feedline Width	w_2	0.77
End-coupled Termination Width	w_3	2.0
Radius of Each MRR	r	3.55
MRR Gap	g	1.09
MRR Inter-Space Distance	k	0.3
Feedline Inter-Space Distance	i	1.0

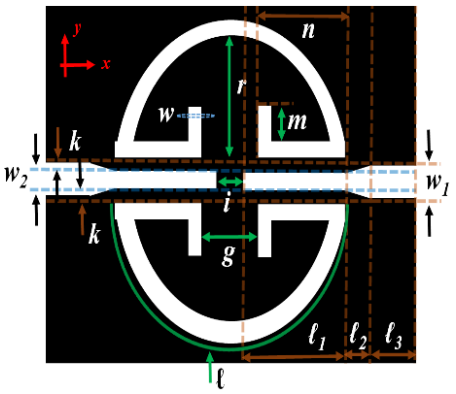

Figure 1: The proposed microstrip-ring resonator.

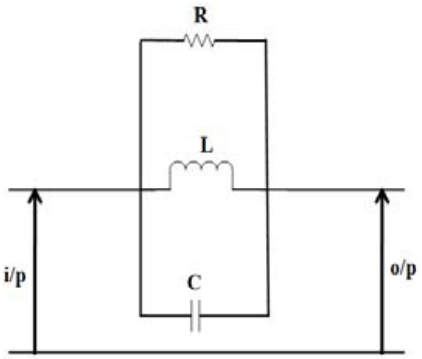

Figure 2: Equivalent circuit of each MRR.

line resonator to a higher frequency such that interference can be minimized. Equations (1)–(3) [11] serve to determine the MRR equivalent circuit inductor, resistor and capacitor value,

$$L = \frac{1}{4\pi^2 f_0^2 C} \tag{1}$$

$$C = \frac{\omega_C}{2Z_O\left(\omega_O^2 - \omega_C^2\right)} \tag{2}$$

$$R = \frac{2Z_O}{\sqrt{\frac{1}{|S_{11}(\omega_O)|^2} - \left(2Z_O\left(\omega_O C - \frac{1}{\omega_O L}\right)\right)^2 - 1}} \tag{3}$$

where ω_0 is angular resonant frequency, ω_c is the lower 3-dB cutoff angular frequency and Z_0 is the scaled impedance of input and output terminated ports. Figure 3 is the Agilent Advanced Design System (ADS) model of the equivalent circuit of the proposed MRR resonator that has been derived. Each half ring (1 and 2) on the lower side of the equivalent circuit represents the two quarter-wave MRRs, whereas the upper side of the equivalent circuit represents the two sides of the end-coupled transmission line, and both are connected to 50 Ω stubs represented by the characteristic impedances Z_0. The two half-rings resonators determine the frequency resonance of the resonator. In this circuit, there are four resonator capacitances, with two on each side labeled accordingly and two feed capacitances. The resonator capacitances are labeled C_{RL1}, C_{RL2} for the left-hand side, and C_{RR1} and C_{RR2} for the right-hand side, whereas the feed capacitances are labeled C_{TLL1}, C_{TLL2}, C_{TLR1}, C_{TLR2}, with their respective inductances and resistances labeled as L_{TLL}, L_{TLR}, R_{TLL} and R_{TLR}. The capacitances C_{TLL1} and C_{TLR1} account for the gap capacitance

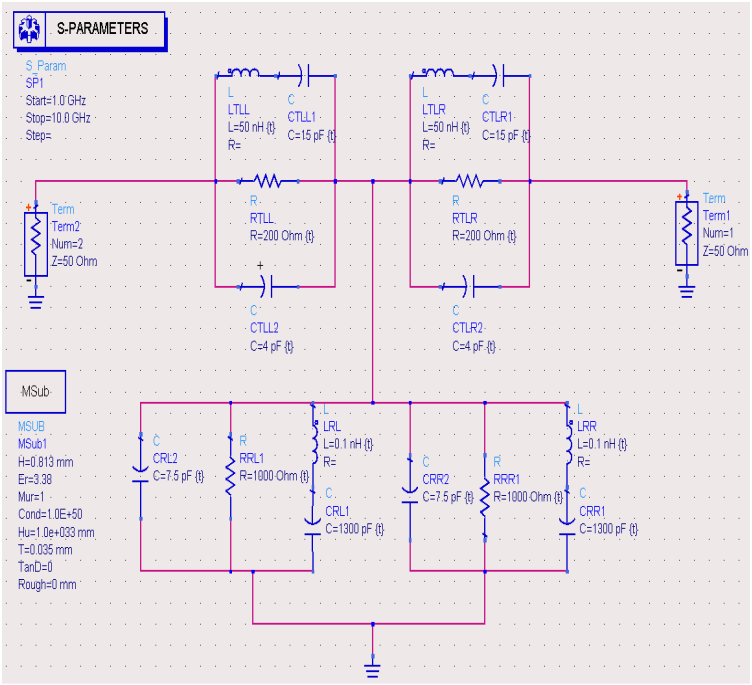

Figure 3: Equivalent circuit model of the proposed MRR resonator using Agilent ADS.

between the lines of distance $0.036\lambda_g$, whereas the line inductances L_{TLL} and L_{TLL}, and the gap capacitances, C_{RL2} and C_{RL1}, are inductances and capacitances between the transmission lines and resonators. The resistances R_{TLL} and R_{TLR} account for the losses. The two end sections of microstrip line that make up the end-coupled transmission line are used to compensate for the phase response in the proposed structure.

Varying the edge gap (k) ensures good coupling with the intent of improving the $|S_{11}|$. The Agilent ADS equivalent circuit modeling of the proposed resonator below demonstrates that each half-ring resonator of the resonators identified in Figure 1 as resonator 1 and 2 introduces one resonant frequency, as mentioned above, and the same frequency can be varied by tuning its respective circuit components to obtain the same resonance in order to ensure high rejection such as attainable in higher-order filters. If both frequencies exhibit a significant differential, then the proposed design will be suitable for wideband applications. Alternatively, if the frequency differential is so significant that there is no overlap between these two frequencies, this may lead to dual-band characteristics. In summary, the symmetrical properties of these resonators are essentially to produce two resonant frequencies, but close to each other. The two resonators control the resonant frequency of the MRR and the characteristic impedance Z_0 of the transmission line is normalized to $50\,\Omega$. The C_{TLL1}, and C_{TLL2} (the capacitances that result from the gap between the lines) were tuned using Agilent ADS until the design resonated at the designed frequency, and their values were extracted from the model. Similarly, L_{TLL} and L_{TLR} (the inductances due to the length of

Table 2: Effect of resonator capacitances and resistances on the MRR performance.

	Resonator Capacitances C_{RL2}, C_{RR1}					**Resonator Resistances** R_{RL1}, R_{RR1}					
SN	**C (pF)**	S_{21} **(dB)**	S_{11} **(dB)**	f_0 **(GHz)**	**BW (MHz)**	**R (kΩ)**	**R (kΩ)**	S_{21} **(dB)**	S_{11} **(dB)**	f_0 **(GHz)**	**BW (MHz)**
1.	4.5	−0.454	−26.86	7.48	730	1	1	−0.475	−27.14	5.8	432
2.	5.5	−0.461	−26.96	6.77	594	0.7	0.7	−0.654	−23.97	5.8	441
3.	6.5	−0.468	−27.05	6.23	501	0.4	0.4	−1.087	−19.30	5.8	441
4.	7.5	−0.475	−27.14	5.8	432	0.1	0.1	−3.631	−9.57	5.8	622
5.	8.5	−0.481	−27.23	5.45	380						

the transmission lines), C_{RL1}, C_{RL2} (the capacitances due to the gap between the microstrip-ring resonators and the transmission lines), and the resistors (R_{TLL}, R_{TLR}, R_{RL1}, and R_{RR1}), which represent the losses in the design as a result of copper loss, were investigated and their values were found to be as tabulated in Tables 1 and 2.

3. RESULTS AND DISCUSSION

Figure 4 shows the Agilent ADS model result. In order to obtain an accurate measurement of the scattering parameters of the resonator, the through-reflect-load calibration was used. The input and output port of the prototype resonator was soldered with an SMA connector and measured using the Agilent E8364B network analyzer. The simulated insertion and reflection coefficient are -0.94 dB and -19.4 dB respectively, whereas the measured insertion loss is -2.76 dB with a reflection coefficient of -11.2 dB at a center frequency of 5.86 GHz. There is reasonable agreement between the simulated and measured results. The connector mismatches and conductor losses are responsible for the dissimilarities. To improve the resonator performance, a low loss tangent laminate board with high dielectric constant substrate material will be adequate and practical to achieve more compact size and lower insertion loss. Considering both the ADS and CST results (though CST results are not shown), the finite integration technique (FIT)-CST simulation result shows similar patterns for the insertion and reflection coefficient, and these are largely influenced when varying the edge gap, (k) parameter. The reflection coefficient depreciates as the edge gap (k) increases and improves otherwise. The insertion loss pattern due to the different end coupled and microstrip-ring resonator edge gap (k) is the opposite. By decreasing the edge gap, a high insertion loss was obtained. The analysis of the edge gap (k), shows its major influence on the resonant frequency of the proposed design. The edge gap (the distance between the feed line and MRR) significantly affects the coupling performance. It is therefore in order to say that there is an inherent relationship between the edge gaps, insertion loss $|S_{21}|$, and reflection coefficients $|S_{11}|$. To establish this, four values of the edge gap are chosen between 0.1 and 0.7 with an incremental value of 0.2 mm using the FIT-CST commercial solver. The effect of these edge gap values was analyzed. It was observed that the responses of $|S_{11}|$ and $|S_{21}|$ were shifted to the higher frequency rather than where they were originally designed after the edge gap was increased, and decreased otherwise. Alternatively, the bandwidth of the proposed design became smaller when the gap between the end-coupled line and MRR became smaller, whereas the bandwidth became wider and the insertion loss improved otherwise. Therefore, by adjusting the gap sizes, the desired values of the insertion loss and resonant frequency can be achieved. Hence, tuning is a possibility and so the proposed resonator offers a degree of design flexibility.

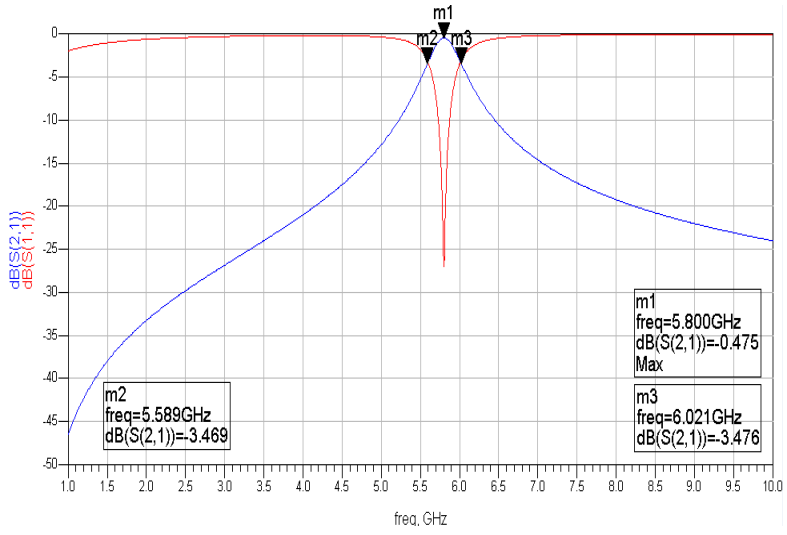

Figure 4: Agilent ADS modeled S-parameter.

4. VALIDATIONS

Figure 4 depicts the ADS modeling of the proposed MRR resonator, as mentioned earlier, whereas Figure 5 represents the respective effects of C_{RR1}, C_{RL2}, R_{RL1}, and R_{RL2} on the reflection coef-

ficient, insertion loss and the bandwidth at a resonant frequency of 5.8 GHz. In Figure 5(a), the insertion loss ($|S_{21}|$) was -0.475 dB with a reflection coefficient ($|S_{11}|$) of -27.14 dB at 7.5 pF resonator capacitances. The resonator capacitances C_{RR1}, and C_{RL1} are the resonator first right and left capacitances, which are equal in value. It was observed that these capacitances are inversely proportional to the modeled results $|S_{11}|$, $|S_{12}|$, the resonant frequency (f_0), and the bandwidth. The higher these capacitances, the better they are for achieving our objectives of narrow bandwidth of close to 5% ($432/5800 \times 100 = 7.45\%$), lower $|S_{21}|$, and good $|S_{11}|$. The effect of varying these capacitances significantly affects both the insertion loss and the resonant frequency in two major ways, namely: 1) the $|S_{21}|$ improved from the current -0.475 to -0.454 dB with a reduced $|S_{11}|$ and wider bandwidth of about 730 MHz, constituting a 12.5% increase.

Unfortunately, the percentage is too high to be considered as narrow bandwidth and thus defeats the FBW design consideration; 2) the $|S_{21}|$ depreciates from the current value to -0.481 dB with an enhanced $|S_{11}|$ of -27.23 dB at a capacitance value of 8.5 pF. The bandwidth is narrower and is put at 380 MHz, but at a frequency of 5.45 GHz. It is therefore noteworthy that the resonant frequency shifts from the designed value as these capacitances vary. Figure 5(b) shows the effect of the first resonators' resistances (R_{RL1} & R_{RR1}) on the $|S_{11}|$, $|S_{21}|$, and the bandwidth. It is evident from the figure that while their effect on the bandwidth is insignificant until somewhere at about 0.4 kΩ, the bandwidth response subsequently becomes steep, such that decreases in the resistances become proportional to the increase in the bandwidth. The $|S_{21}|$ improves marginally until 0.4 kΩ, where the responses become very significant but depreciable $|S_{11}|$.

In Figure 6, the effect of the second resonator capacitances and inductances on the resonator performances is presented. The effect of the resonator inductances as depicted in Figure 6(a) indi-

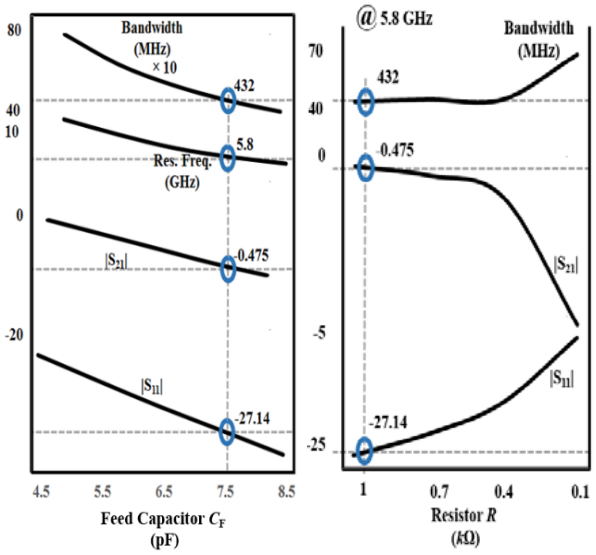

Figure 5: Effect of 1st resonator capacitances and inductances.

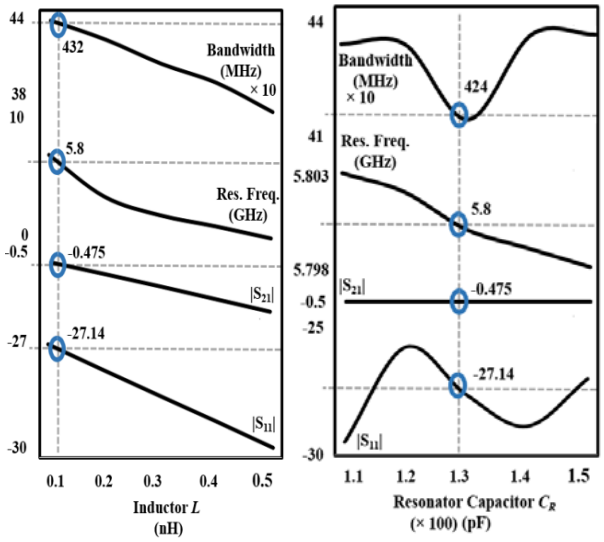

Figure 6: Effect of 2nd resonator capacitances and resistors.

Table 3: Effect of resonator capacitances and inductances on the MRR performance.

SN	Resonator Inductances L_{RL}, L_{RR}					Resonator Capacitances C_{RL1}, C_{RR2}				
	L (nH)	**S_{21} (dB)**	**S_{11} (dB)**	**f_0 (GHz)**	**BW (MHz)**	**C ($\times 10^3$ pF)**	**S_{21} (dB)**	**S_{11} (dB)**	**f_0 (GHz)**	**BW (MHz)**
1.	0.1	−0.475	−27.14	5.800	432	1.1	−0.475	−27.144	5.803	432
2.	0.2	−0.527	−27.86	4.082	424	1.2	−0.475	−27.138	5.802	432
3.	0.3	−0.580	−28.56	3.318	414	1.3	−0.475	−27.141	5.800	424
4.	0.4	−0.635	−29.26	2.862	405	1.4	−0.475	−27.143	5.799	433
5.	0.5	−0.690	−29.97	2.365	394	1.5	−0.475	−27.140	5.798	433

cates that all the design parameters ($|S_{11}|$, $|S_{21}|$, and BW) improve considerably with increases of the resonator inductance, as shown in Table 2. However, the design frequency changes progressively as the inductance values increase. The effect of the second resonator capacitances on these performance parameters is marginal, as shown in Table 3. The $|S_{21}|$ is constant, as shown in Figure 6(b), but with a marginal observable variance in $|S_{11}|$ as well as BW. The resonant frequency variance is also marginal.

5. CONCLUSION

In this paper, a novel compact narrowband resonator based on the MRR using a dual half-ring is presented. The entire structure was investigated using a numerical solver such as the 2D equivalent circuit Agilent ADS modeler. The derived equivalent circuit model has been validated by both an analytical solution and numerical simulations. The resulting model was then tuned to the designed frequency and the circuit parameter values were subsequently extracted and analyzed. The simulated results were compared with the modeled ones and experimental data and reasonable agreements were demonstrated. The proposed design presents apparent size reduction, compared to many reported conventional parallel-coupled or end-coupled microstrip resonators (though not reported in this work for the sake of brevity), with reasonable performance enhancement.

REFERENCES

1. Rashidian, A., M. T. Aligodarz, and D. M. Klymyshyn, "Dielectric characterization of materials using a modified microstrip ring resonator technique," *IEEE Transactions on Dielectrics and Electrical Insulation*, Vol. 19, No. 4, 1392–1399, August 2012.
2. Hopkins, R. and C. Free, "Equivalent circuit for the microstrip ring resonator suitable for broadband materials characterisation," *IET Microwaves, Antennas & Propagation*, Vol. 2, No. 1, 66–73, Feb. 2008.
3. Bernard, P. A. and J. M. Gautray, "Measurement of dielectric constant using a microstrip ring resonator," *IEEE Transactions on Microwave Theory and Techniques*, Vol. 39, No. 3, 592–595, Mar. 1991.
4. Kim, C.-S., D.-H. Kim, I.-S. Song, K. M. K. H. Leong, T. Itoh, and D. Ahn, "A design of a ring resonators with wide rejection band using DGS and spur-line coupling structures," *IEEE MTT-S International Microwave Symp. Dig.*, 412–417, Jun. 2005.
5. Mandal, S., H. O. Roy, L. B. Dubey, and A. K. Shukla, "Design and development of band pass resonator at 140 GHz," *International Conf. on Recent Advances in Microwave Theory and Applications, MICROWAVE 2008*, 255–257, Nov. 2008.
6. Yu, Z. and Q. Wang, "A multi-band small antenna based on deformed microstrip ring resonators of left-handed meta-materials," *International Symp., Microwave, Antenna, Propagation and EMC Technologies for Wireless Communications*, 531–534, 2007.
7. Bin, Z. and S. Uysal, "An accurate design technique for microstrip edge-end-coupled resonators," *Microwave and Optical Technology Lett.*, Vol. 18, No. 4, Jul. 1998.
8. Choi, J. and C. Seo, "Low phase noise VCO using microstrip square open loop multiple microstrip ring resonator," *IEEE MTT-S International Microwave Symp. Dig.*, 1469–1472, 2008.
9. Janhsen, A., B. Schiek, and V. Hansen, "On the definition of quasi lumped elements in planar microwave circuits," *22nd European Microwave Conference, 1992*, Vol. 1, 251–256, Sep. 5–9, 1992.
10. Zhang, R., "Novel planar microstrip and dielectric resonator resonator," PhD Thesis, Department of Electrical & Computer Engineering, University of Waterloo, 2007.
11. Lin, X. Q. and T. J. Cui, "Controlling the bandwidth of microstrip ring resonators," *Microwave and Wireless Components Lett.*, Vol. 18, No. 4, 245–247, 2008.